Sensors and Materials, Vol. 22, No. 3 (2010) 121–134
MYU Tokyo

S & M 0794

Detection of Hydrogen and NO_x Gases Based on a Thermoelectric Gas Sensor with an Embedded Tin Oxide Catalyst

Seung-Il Yoon, Chung-Il Lee and Yong-Jun Kim*

Microsystems Laboratory, School of Mechanical Engineering, Yonsei University
Shinchon-dong 134, Seodaemun-gu, Seoul 120-749, Republic of Korea

(Received March 26, 2009; accepted September 8, 2009)

Key words: thermoelectric gas sensor, tin oxide, thermal resistivity layer, hydrogen gas detection, NO_x gas detection

In this paper, we report a micromachined thermoelectric gas sensor with an embedded catalyst that can be used for gas sensing applications. The proposed sensor can detect the target gas by measuring heat from the catalytic reaction on the surface of the catalyst, tin oxide in this case. By using the thermoelectric effect, decreased response and recovery times can be obtained. To increase the sensitivity of the sensor, the thermal components of the proposed gas sensor are fabricated on a high-thermal-resistivity layer, SU-8 in this case, which led to the reduction in the rate of parasitic heat transfer to the substrate. In order to verify the thermal characteristic of the fabricated sensor, the intensity of output signals depending on the temperature differences between the hot and cold junctions was measured. The sensor response to the temperature change was 4.61 V/W. Hydrogen and NO_x gases were detected by the proposed sensor. The change in output signal intensity depending on hydrogen gas concentration was 1.06×10^{-1} μV/ppm, and the change in output signal intensity depending on NO_x gas concentration was 1.50×10^{-1} μV/ppm.

1. Introduction

With increasing interest in air quality, the demand for monitoring or detecting harmful gases has also increased. In particular, the demand for detecting hydrogen and nitrogen oxide (NO_x) gases has increased sharply because the accumulation of these gases, which are air pollutants released from the combustion exhaust of automobile engines, home heaters, furnaces and plants, has become more serious worldwide in recent years.[1]

The major issues in gas sensor research have been classified into two categories, namely, sensing materials and sensing methods. There have been many efforts for improving sensing materials, but with respect to sensing methods, the resistance measurement type dominates over all other sensing methods.[2–4] However, it is difficult to apply it to real-time and continuous detection. Previous investigations on the

*Corresponding author: e-mail: yjk@yonsei.ac.kr

resistance measurement type are based on the measurement of the change in electrical resistance. They require continuous electrical power supply for the measurement, which results in a large electrical power consumption. Moreover, because the resistance measurement type uses a thick catalyst layer, which is good for a higher sensitivity but bad for a faster reaction, response and recovery times are delayed (~min).[5] Furthermore, this measurement type requires complicated fabrication steps and a relatively complex measurement circuitry. For example, metal semiconductor sensors require annealing processes at extremely high temperatures in excess of 400°C,[6] and solid-electrolyte gas sensors require ceramic substrates, such as zirconia-based materials, and annealing processes for activating the substrate.[7]

A thermoelectric gas sensor based on a thermopile would be a strong candidate for effective and inexpensive gas detection because of its easy, reliable working principle and good sensing performance for a wide range of gas concentrations.[8] It can convert temperature change due to the catalytic reaction heat between the catalyst and gas species to an electric signal via the Seebeck effect.[9,10] Furthermore, it does not require an additional measurement circuitry and any power supply because it can detect gas by measuring only the generated electrical potential due to the reaction. Also, by simply changing the catalytic materials used in the device, the user can use this sensor to detect other gases.[11]

The electrical potential measured by the thermoelectric gas sensor is proportional to the temperature difference between the hot and cold junctions of the thermopile. To achieve a high-sensitivity thermoelectric gas sensor, it is important to reduce the rate of heat transfer from the thermopile to the substrate, which is called 'parasitic heat transfer.' In previous studies, diaphragm structures, floating membrane structures or elevated structures of thermoelectric sensing layers were used to minimize parasitic heat transfer.[12,13] However, the use of these structures has downsides, such as the yield reduction of the device due to a complicated bulk-micromachining fabrication process. In particular, elevated thermoelectric gas sensors are fragile to agitations induced by fluctuations in external gas flow and by mechanical shocks.

In this paper, a simple structured thermoelectric gas sensor is proposed. By using a thermopile, the proposed sensor can detect the target gas by measuring the reaction heat between the gas and a thin catalyst film. To improve the sensitivity of the thermoelectric gas sensor by minimizing parasitic heat transfer from the thermopile to the substrate without complex fabrication steps, thermoelectric components were fabricated simultaneously on a high-thermal-resistivity layer. The voltage difference between the two thermopiles, one with a catalytic layer, and the other with a reference thermoelectric layer, was measured using a differential amplifier to eliminate external thermal noise. The proposed gas sensor was fabricated using MEMS technology and characterized by its capability to detect hydrogen and NO_x gases.

2. Materials and Methods

Figure 1 shows the schematic view and sensing principle of the proposed gas sensor. The gas sensor consists of a 100-μm-thick high-thermal-resistivity layer and sensing and

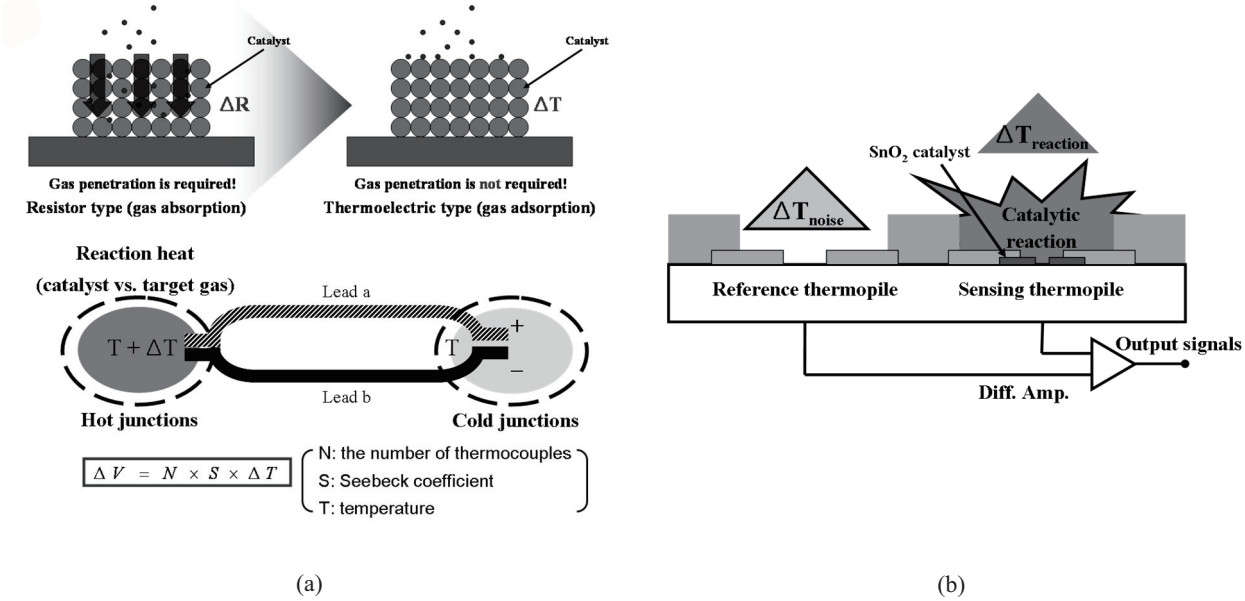

Fig. 1. Conceptual views of the proposed thermoelectric gas sensor: (a) principle of gas sensing based on a thermopile and (b) schematic view of the proposed thermoelectric gas sensor.

reference thermopiles with bismuth and chrome pairs. SnO_2 is used as the catalyst layer, which is embedded under the hot junctions of only the sensing thermopile. Among the different materials studied for gas-sensing applications, SnO_2 was found to be the most appropriate among all the other metal oxides. The gas sensing properties of this material have been widely been reported in the literature. Well-known advantages of this material include its low cost and high sensitivity to different gas species.[14]

The measurement circuit on the printed circuit board (PCB) is integrated with the sensor. The circuit consists of two low-pass filters (LPFs) that filter out electrical noise and a differential amplifier (AD620, Analog Devices, Inc., USA). The cutoff frequency of the designed LPFs is 80 Hz.

Detailed dimensions are as follows: (1) overall dimensions: 28 mm (l)×23 mm (w); (2) width of the thermopile: 50 μm; (3) length of the thermopile: 5 mm; (4) thickness of the bismuth and chrome layers: 1 μm; (5) number of thermocouples: 120; (6) size of the catalyst layer: 150 μm (l) × 200 μm (w)×0.3 μm (h); and (7) thickness of the SU-8 layer: 100 μm (Table 1).

2.1 *Sensing principle*

For the detection of the target gas, a catalyst film is embedded under only the hot junctions of the thermopile. For the removal of thermal noises, a reference thermopile, which has no catalyst layer, is integrated with the sensing thermopile. The differential

Table 1
Geometrical parameters of the thermoelectric gas sensor.

Parameter	Dimension
Overall size	28 mm (l)×23 mm (w)
Width of thermopile	50 μm
Length of thermopile	5 μm
Thickness of thermopile	1 μm
Number of thermocouples	120
Size of catalyst layer	150 μm (l) × 200 μm (w) × 0.3 μm (h)
Thickness of SU-8 (thermal resistivity layer)	100 μm

amplifier can extract the output signal changes due to only the gas reaction.

When the target gas is adsorbed by the catalyst surface, reaction heat due to the catalytic reaction between the gas and the catalyst surface is generated immediately, as shown in eq. (1), and the generated reaction heat increases in temperature at the hot junctions. By measuring this temperature change at the hot junctions and using eq. (2), the target gas can be detected.

$$\begin{aligned} NO_{2,gas} &\leftrightarrow NO_{2,ads} + \text{reaction heat} \\ H_{2,gas} &\leftrightarrow H_{2,ads} + \text{reaction heat} \end{aligned} \quad (1)$$

$$\Delta V = n \times R \times \Delta T \ (n = 1, 2, 3...) \quad (2)$$

ΔV: output voltage
n: number of thermocouples
R : difference in Seebeck coefficient between materials that compose thermopile
ΔT : temperature difference between hot and cold junctions

The integrated Seebeck coefficient of 120 thermocouples ($n \times R$) is 11.6 $mV \cdot K^{-1}$. Because the temperature difference is proportional to the amount of reaction heat, linear output signals can be obtained depending on the gas concentrations.

2.2 *High thermal resistivity layer for sensor sensitivity increase*

We propose a high-thermal-resistivity layer of SU-8 (SU-8 2100, MicroChem. Corp., USA) for the insertion between the substrate and the thermoelectric components. By using only the SU-8 layer instead of a bulk-micromachined structure, parasitic heat transfer can be minimized.

Thermal energy due to the catalytic reaction is transferred to the substrate and the thermal sensing component simultaneously. To increase the sensitivity of the sensor, it is important to concentrate the thermal energy transfer to only the thermal sensing component. This means that the parasitic heat transfer to the substrate must be minimized.

The relationship between the rate of parasitic heat transfer to the substrate per temperature change and the thermal conductivity of the substrate can be expressed by eqs. (3)

and (4),[15] and Fig. 2 shows a simplified thermal modeling.

$$R_T = L/(k \cdot A) \tag{3}$$

R_T: thermal resistance (°C/W)
L: thickness of layer (m)
k: thermal conductivity of layer (W/m·°C)
A: area of layer (m_2)

$$\dot{q} = \frac{q}{\Delta T} = \frac{1}{R_{T1} + R_{T2}} \tag{4}$$

$\dot{q}$: rate of heat transfer per temperature change (W/°C)
q: rate of heat transfer (W)
ΔT: temperature difference (°C)
R_{T1}: thermal resistance of SU-8 layer (°C/W)
R_{T2}: thermal resistance of silicon substrate (°C/W)

The thicknesses (L) of the silicon substrate and the SU-8 layer were 500 and 100 μm, respectively. The area (A) of each layer was 15 mm^2, which was the same as that of the catalyst layer region. The thermal conductivities (k) of silicon and SU-8 were 130 and 0.15 W/m·°C, respectively. Using eq. (3), the thermal resistances of the SU-8 layer (R_{T1}) and the silicon substrate (R_{T2}) were calculated to be 33.33 and 0.26 °C/W, respectively. At the same time, the rate of the parasitic heat transfer to the substrate per temperature change was 3.85 W/°C when only the silicon substrate was used. On the other hand, when the SU-8 layer was used as the thermal resistivity layer, the rate of parasitic heat transfer to the substrate per temperature change was calculated to be 0.03 W/°C by eq. (3), which is 0.8% of that obtained with the use of only the silicon substrate.

It was also important to consider the thermal conductivity of the thermopile itself since its high thermal conductivity reduced the temperature difference between the hot

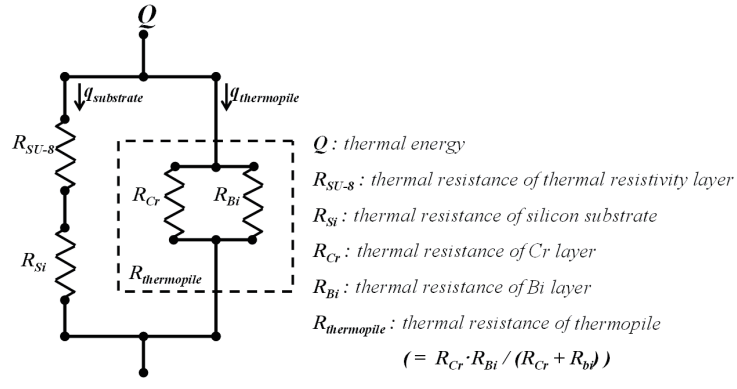

Fig. 2. Thermal analysis of the proposed sensor: a simplified thermal modeling.

and cold junctions. In this study, the thermopile composed of 120 thermocouples had a width of 50 μm, a thickness of 1 μm, and a length of 5 mm, and thermal conductivities of Cr and Bi were about 94 and 8 W/m°C, respectively. By using these parameters and eq. (3), thermal resistances of Cr and Bi layers were calculated to be 88,652 and 104,1667 °C/W. Thus, the thermal resistance of the thermopile was calculated to be 81,700 °C/W, and the rate of heat transfer per temperature change through the thermopile was 1.22×10^{-5} W/°C, which was much less than that in the case of the substrate previously mentioned. Although the thermal conductivity of the thermopile was higher than that of the substrate, heat loss through the thermopile was insignificant because the length of the thermopile was large and its cross-sectional area was very small. Thus, the thermal conductivity of the thermopile was negligible.

To verify the result of the calculation, a computational simulation using Fluent 6.0 (Fluent Inc., USA) was carried out. Figure 3 shows the results of the simulation. From these results, it was observed that when the thermal resistivity layer was used, the parasitic heat transfer to the substrate was completely prevented because the thermal component was thermally isolated.

2.3 *Fabrication of the thermoelectric gas sensor*

All components of the proposed thermoelectric gas sensor were produced using only surface micromachining techniques. Figure 4(a) shows the simplified fabrication process. Optical photographs of the fabricated microcalorimeter and its package are shown in Fig. 4(b).

First, a 100-μm-thick SU-8 layer is spin-coated on a Pyrex wafer to obtain a high-thermal-resistivity layer. Second, a 2.3-μm-thick photoresist is spin-coated on the SU-8 layer and patterned to define the catalyst pattern, and then, a 0.3-μm-thick SnO_2 layer is formed on the Pyrex substrate using a thermal evaporator and the lift-off process. The tin oxide catalyst layer is sintered at 300°C for 3 h. After this patterning, a 1-μm-thick Ti-

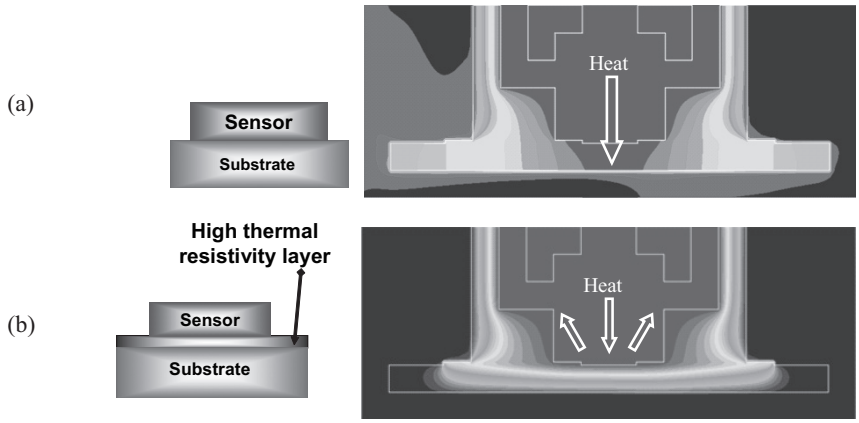

Fig. 3. Thermal analysis of the proposed sensor using Fluent: (a) computational simulation result when only the silicon substrate is used and (b) computational simulation result when the high-thermal-resistivity layer is used with the silicon substrate.

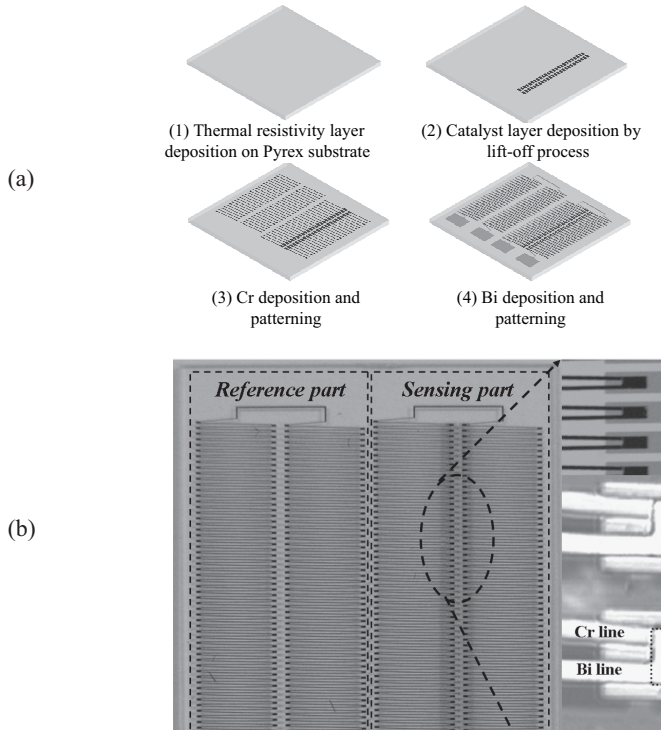

Fig. 4. (a) Simplified fabrication process for the proposed thermoelectric gas sensor using 4 masks and (b) optical views of the fabricated thermoeletric gas sensor.

Bi layer is deposited on the SU-8 layer using a sputtering system and is patterned. Ti is used to fabricate the adhesion layer for the Bi deposition. A 1-μm-thick Cr is deposited and patterned as crossed with Ti-Bi patterns. By these metal patterning processes, the thermopile composed of 120 Bi-Cr pairs is realized. The hot junctions of the sensing thermopile are defined on the catalyst layer.

3. Results and Discussion

3.1 *Thermal characteristics of the proposed thermoelectric gas sensor*

To determine the thermal characteristics of the proposed sensor, output signals that depend on the temperature difference between the cold and hot junctions were measured for N_2 gas. N_2 gas at temperatures from 5 to 35°C higher than room temperature was injected to only the hot junctions of the sensing thermopile, and the output voltage changes due to the applied heat were measured.

The applied heat and the thermal sensitivity of the sensor can be calculated using eqs. (5) and (6). The thermal sensitivity means output voltage change per applied heat. It is a constant value determined by the sensor design and can be converted to output voltage per unit temperature change.

$$q = C \times \dot{m} \times \Delta T \quad (5)$$

q: applied heat (W)
$\dot{m}$: mass flow rate of N_2 gas (g/s)
ΔT: temperature difference (°C)
C: specific heat ($cal \cdot g^{-1} \cdot °C^{-1}$)

$$\text{Thermal sensitivity} = \Delta V / q \quad (6)$$

Thermal sensitivity: output voltage change per applied heat (V/W)
ΔV: measured output voltage depending on temperature difference between junctions (V)

The thermal sensitivity of the sensor was 4.61 V/W (= 3.01 mV/°C) depending on the temperature difference between the hot and cold junctions, as shown in Table 2 and Fig. 5. This value was lower than the designed value (11.60 $mV/°C^{-1}$) mentioned in § 2.1, because there was still heat loss to the air and substrate even when a thermal resistivity layer was used. However, from this comparison, we could state that the fabricated sensor performance and the measurement process were valid for a gas sensing application.

3.2 *Detection of hydrogen and NO_x gases*

The fabricated gas sensor was characterized by its capability to detect hydrogen and NO_x gases. Figure 6 shows the measurement setup. Three gases, namely, N_2, H_2, and NO_2, were used for the measurement. N_2 gas was used as the reference gas. H_2 and NO_2 were used as the target gases and were in a specific concentrated mixture with N_2 gas. The concentration of each gas was precisely controlled using a mass flow controller (100 ml/min). By using a heat exchanger and an environmental chamber (60 cm (w)×50 cm (l)×50 cm (h)), the surroundings of the sensor and the injected gases were maintained at fixed temperature and humidity. In the environmental chamber, the fabricated sensor was loaded into a reaction chamber of acryl (3 cm (w)×5 cm (l)×3 cm (h)), which was directly connected to the heat exchanger by a pipe. The temperature of the substrate was monitored by a commercial precision temperature sensor (LM35, National Semiconductor Corp., USA). The output signal changes due to the catalytic reaction between the target gases and the SnO_2 catalyst were recorded by an I-V meter (Semiconductor Characterization System 4200, Keithley).

Table 2
Output signals of the proposed gas sensor depending on temperature differences between hot and cold junctions.

Temperature difference (°C)	Applied thermal energy (mV)	Measured output voltages (mV)		Thermal sensitivity (V/W)
		Average	Standard variation	
5	178.04	12.38	1.35	4.51
15	534.12	35.38	1.52	4.29
25	890.20	68.94	3.41	5.02
35	1246.28	81.96	2.75	4.26

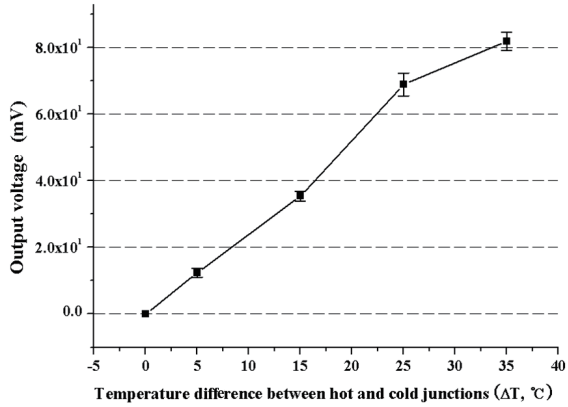

Fig. 5. Output voltage changes depending on temperature differences between the hot and cold junctions. The thermal sensitivity of the sensor was 3.01 mV/°C (= 4.61 V/W) depending on the temperature difference between the hot and cold junctions. The result shows good linearity to the temperature.

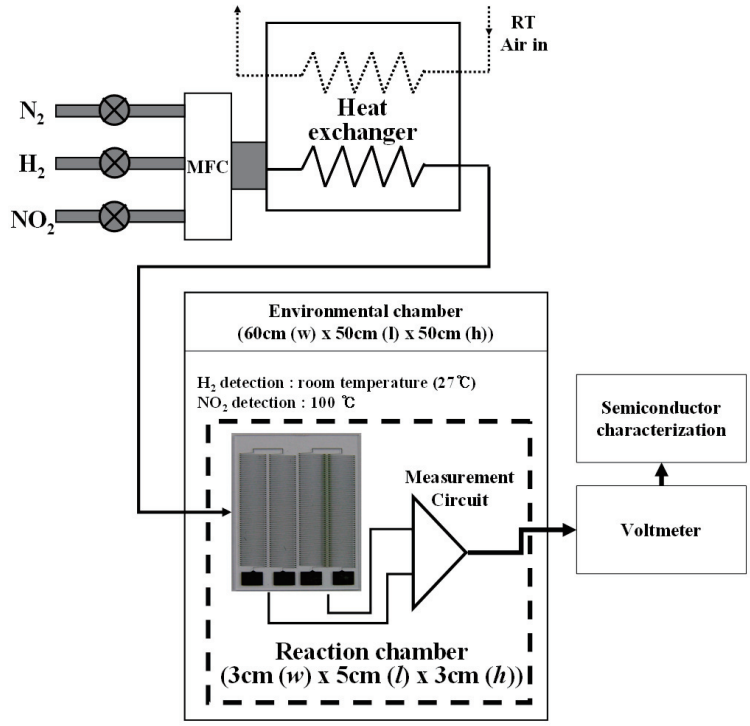

Fig. 6. Measurement setup.

Initially, the reference gas, dehydrated N_2 gas, was supplied into the chamber at a constant flow rate. During this step, the output voltages changed slightly owing to the gas flow itself. This noise was compensated for by comparing the output voltages between the sensing and reference thermopiles. Then, the reference gas was switched to the target gases, and the target gases of various concentrations were introduced into the chamber. After a specific time had elapsed for gas reaction, the reference gas was resupplied into the chamber instead of the target gases. All experiments were performed several times, and no chemical or physical alterations of the catalyst were observed.

3.2.1 *Hydrogen gas detection*

The concentration of the hydrogen gas was varied from 1,000 to 10,000 ppm. The operating temperature of the sensor was room temperature (27°C). Figure 7 shows the response of the thermoelectric gas sensor to 1,000 ppm hydrogen gas in N_2 gas. When

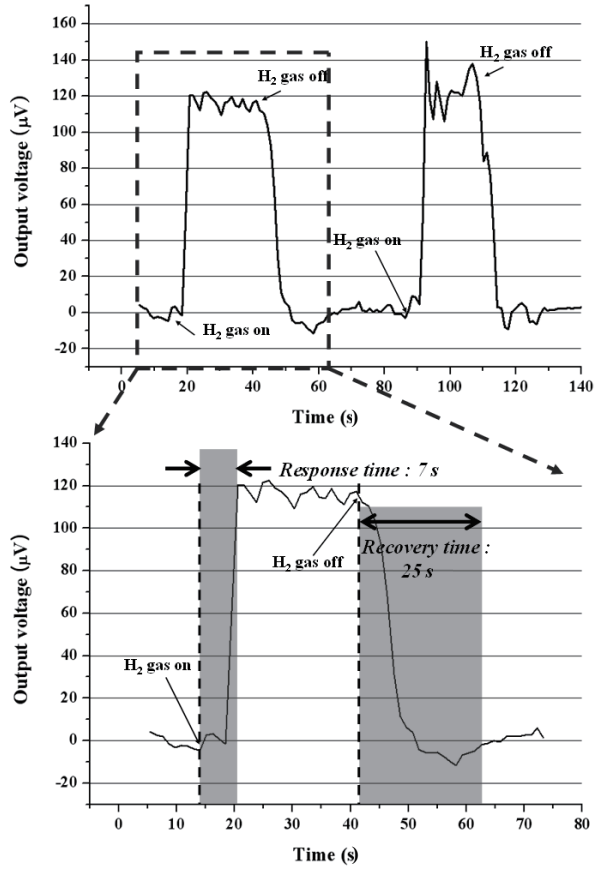

Fig. 7. Measured output voltages during detection of 1,000 ppm hydrogen gas. When the hydrogen gas of the same concentration was resupplied into the reaction chamber, a very similar pattern of ΔV was reproduced. The response and recovery times were 7 and 25 s, respectively.

the hydrogen gas was introduced into the reaction chamber, the output voltage ΔV of the sensor increased markedly and then reached the steady state. ΔV saturated at about 115 μV in just 7 s (= response time, which is defined as the arrival time to 90% of the average of the differences from the starting level to the target level). Then, ΔV recovered to its initial value, near the zero level, only 25 s after the hydrogen gas supply was stopped (= recovery time). When the hydrogen gas of the same concentration was resupplied into the reaction chamber, a very similar pattern of ΔV was reproduced. The recovered zero level voltage was very stable and no conspicuous drift was observed. This indicated that the reaction heat generated by the catalytic reaction reached thermal equilibrium with the heat loss to the surroundings of the sensor, such as the flow of the injected gases and substrate. During the experiment, no temperature changes of the substrate were observed. Figure 8(a) shows the output signal change depending on the hydrogen

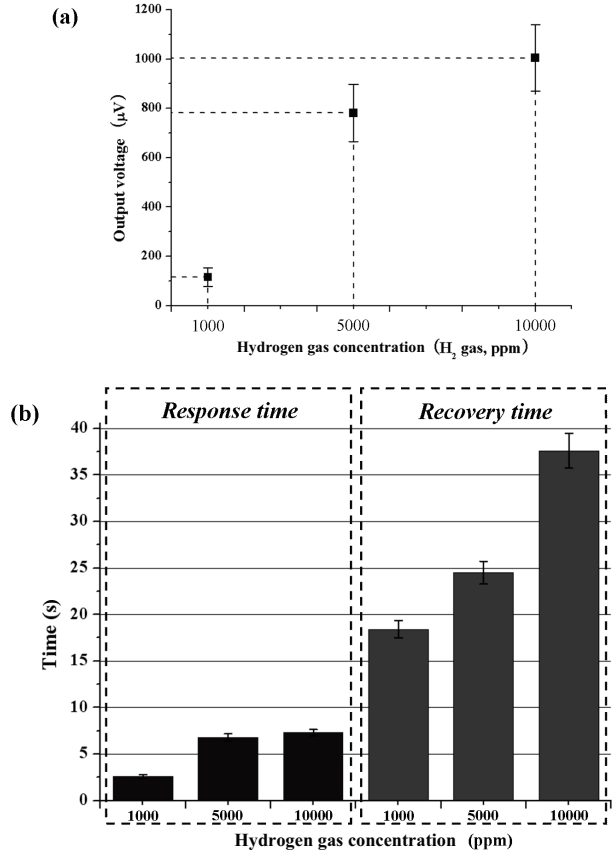

Fig. 8. Results of hydrogen gas detection. (a) Output signal change depending on the hydrogen concentration. The sensitivity of the proposed sensor for hydrogen gas detection was measured to be 1.06×10^{-1} μV/ppm. (b) The response and recovery times of the proposed sensor depending on hydrogen concentration were much less than those of the previous resistance measurement type.

concentration. The sensitivity of the proposed sensor for hydrogen gas detection was measured to be 1.06×10^{-1} μV/ppm. Figure 8(b) shows the response and recovery times depending on hydrogen gas concentration.

3.2.2 *NO_x gas detection*

The experimental process for NO_x gas detection was almost the same as that for hydrogen gas detection. NO_2 gas of various concentrations from 100 to 1,000 ppm was used. The operating temperature of the sensor was 100°C, which was the temperature required to activate the catalyst layer. Figure 9 shows the sensor response for 1,000 ppm NO_x gas in N_2 gas. When 1,000 ppm NO_x gas was introduced into the reaction chamber, output voltage saturated at about 100 μV. Figure 10(a) shows the output signal change depending on NO_x gas concentration. The sensitivity of the proposed sensor for NO_x gas detection was measured to be 1.50×10^{-1} μV/ppm. Figure 10(b) shows the response and recovery times depending on NO_x gas concentration. The response and recovery times were shorter than 1 min.

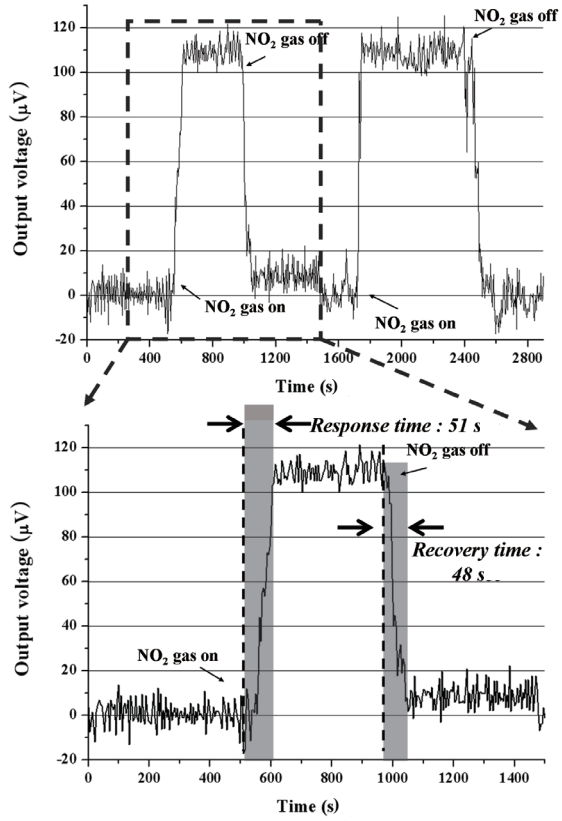

Fig. 9. Measured output voltages during detection of 1,000 ppm NO_x (NO_2) gas. When the 1,000 ppm NO_x gas was introduced to the reaction chamber, the output voltage became saturated at about 100 μV, and the response and recovery times were 51 and 48 s, respectively.

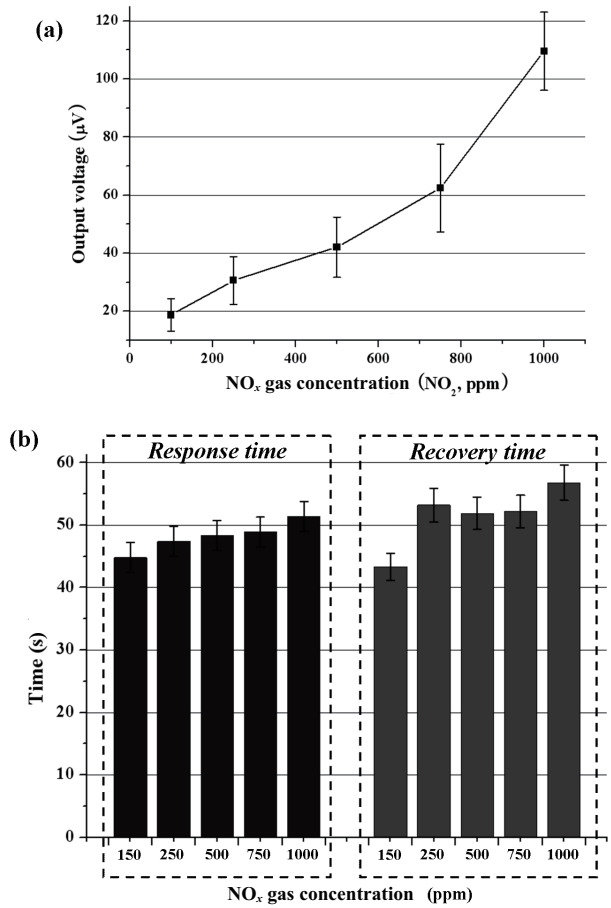

Fig. 10. Results of the NO_x (NO_2) gas detection. (a) The output signal change depending on NO_x gas concentration was 1.5×10^{-1} μV/ppm. (b) The response and recovery times of the proposed sensor depending on NO_x gas concentration were shorter than 1 min.

4. Conclusion

A thermoelectric gas sensor was designed and fabricated for the simple and fast detection of hydrogen and NO_x gases. Previous gas detection research studies have focused on high sensitivity, good selectivity, and fast detection. Improvements in the sensitivity and selectivity of the sensor can be achieved depending on the type of catalyst used. With respect to the detection method itself, the improvement in detection time has emerged as an important issue. In the case of the resistance measurement type based on a thick catalyst layer, the gas absorption process requires 5–7 min at least, which makes fast response and recovery impossible. Therefore, we propose a novel gas sensing method based on a thermoelectric device for real-time detection. By using

a thin catalyst film, response and recovery times markedly improved, and operating temperature decreased. The fabricated gas sensor was characterized by its capability to detect hydrogen and NO_x gases. In H_2 and NO_x gas detection, the measured response and recovery times (~s) were much less than those of the previous gas sensors (~min). By using a reference thermopile, various noises, such as the temperature of the air and a drift in the intensity of the sensor signal due to gas flow, were compensated for automatically without any power consumption or thermal calibration step. The proposed sensor has not only simple structure and measurement process, but also good integration compatibility with other components for gas detection and gas property analysis. Therefore, it can be applied in various fields, such as lab-on-a-chip design.

Acknowledgements

This research was supported by the National Research Foundation of Korea under the National Core Research Center for Nanomedical Technology (R15-2004-024-00000-0) and the Ministry of Knowledge Economy, Korea, under the Information Technology Research Center (ITRC) support program supervised by the Institute of Information Technology Assessment (IITA) (IITA-2009-C1090-0902-0038).

References

1 Ch. Y. Wang, M. Ali, Th. Kups, C.-C. Rohlig, V. Cimalla, Th. Stauden and O. Ambacher: Sen. Actuators, B **130** (2008) 589.
2 J. Tamaki, J. Niimi, S. Ogura and S. Konishi: Sen. Actuators, B **117** (2006) 353.
3 S. Shukla, P. Zhang, H. J. Cho, S. Seal and L. Ludwig: Sen. Actuators, B **120** (2007) 573.
4 E. Comini: Anal. Chim. Acta **568** (2006) 28.
5 A. Gurlo, N. Barsan, M. Ivanovskaya, U. Weimar and W. Gopel: Sen. Actuators, B **47** (1998) 98.
6 X. He, J. Li, X. Gao and L. Wang: Sen. Actuators, B **93** (2003) 463.
7 E. Billi, J. Viricelle, L. Montanaro and C. Pijolat: IEEE Sens. J., **2** (2002) 342.
8 V. Casey, J. Cleary, G. D'Arcy and J. B. McMonagle: Sen. Actuators, B **96** (2003) 114.
9 K. Ramanathan, M. Khayyami and B. Danielsson: Immunobiosensors based on Thermistors, Method iin Biotechnology Affinity Biosensors: Techniques and Protocols, 7 (Humana Press, London, 1998) pp. 19–29.
10 A. E. Beezer: Biological Microcalorimetry (Academic Press, London, New York, 1980).
11 M. Wu and A. Micheli: Sen. Actuators, B **100** (2004) 291.
12 W. Winter and G. W. H. Hohne: Thermochim. Acta **403** (2003) 43.
13 Y. Zhang and S. Tadigadapa: Biosens. Bioelectron. **19** (2004) 1733.
14 G. Eranna, B. C. Joshi, D. P. Runthala and R. P. Gupta: Critical Reviews in Solid State and Materials Sciences in Oxide Materials for Development of Integrated Gas Sensors—A Comprehensive Review (Taylor & Francis, London, 2004) pp. 137–141.
15 J. W. Dally: Packaging of Electronic Systems (McGraw-Hill Inc., New York, 1990) pp. 302–311.